

Pressure-induced structures of Si-doped HfO₂

Chris M. Fancher, Lili Zhao, Matthew Nelson, Ligang Bai, Guoyin Shen, and Jacob L. Jones

Citation: *Journal of Applied Physics* **117**, 234102 (2015); doi: 10.1063/1.4922717

View online: <http://dx.doi.org/10.1063/1.4922717>

View Table of Contents: <http://scitation.aip.org/content/aip/journal/jap/117/23?ver=pdfcov>

Published by the [AIP Publishing](#)

Articles you may be interested in

[Photo-induced tunneling currents in MOS structures with various HfO₂/SiO₂ stacking dielectrics](#)

AIP Advances **4**, 047112 (2014); 10.1063/1.4871407

[Crystal structure of Si-doped HfO₂](#)

J. Appl. Phys. **115**, 034104 (2014); 10.1063/1.4861733

[The structural and electronic properties of HfO₂](#)

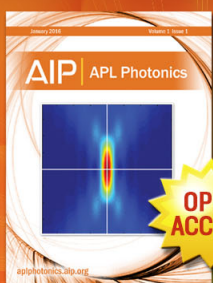
AIP Conf. Proc. **1447**, 1077 (2012); 10.1063/1.4710380

[Influence of Ti substitution on the electrical properties of metal-ferroelectric \(BiFeO₃\)-insulator \(HfO₂\)-silicon structures for nonvolatile memory applications](#)

J. Appl. Phys. **109**, 091604 (2011); 10.1063/1.3581202

[Pressure-induced cubic-to-orthorhombic phase transformation in the negative thermal expansion material HfW₂O₈](#)

J. Appl. Phys. **89**, 3184 (2001); 10.1063/1.1347412



Launching in 2016!

The future of applied photonics research is here

OPEN ACCESS

AIP | APL Photonics

Pressure-induced structures of Si-doped HfO₂

Chris M. Fancher,¹ Lili Zhao,^{1,2} Matthew Nelson,¹ Ligang Bai,³ Guoyin Shen,³ and Jacob L. Jones^{1,a)}

¹Department of Materials Science and Engineering, North Carolina State University Raleigh, North Carolina 27695, USA

²School of Information Science and Technology, Northwest University, Xi'an 710127, China

³HPCAT, Geophysical Laboratory, Carnegie Institution of Washington, Argonne, Illinois 60439, USA

(Received 4 April 2015; accepted 6 June 2015; published online 18 June 2015)

The effect of hydrostatic pressure on the structure of Si-doped HfO₂ (Si:HfO₂) was studied by using a diamond anvil cell in combination with high-energy X-ray diffraction at a synchrotron source. Diffraction data were measured *in situ* during compression up to pressures of 31 GPa. Si:HfO₂ with 3, 5, and 9 at. % Si were found to undergo a monoclinic to orthorhombic transition at pressures between 7 and 15 GPa. Whole pattern analysis was carried out using nonpolar (*Pbca*) and polar (*Pca2*₁) crystallographic models to investigate the symmetry of the observed high-pressure orthorhombic phase. Rietveld refinement results cannot discriminate a reliable difference between the *Pbca* and *Pca2*₁ structures as they nearly equally model the measured diffraction data. The pressure dependent lattice parameters, relative volume, and spontaneous strain are reported.

© 2015 AIP Publishing LLC. [<http://dx.doi.org/10.1063/1.4922717>]

INTRODUCTION

Ferroelectric materials are used for a wide variety of applications such as nonvolatile memories, sonar, ultrasound, actuators, and energy harvesting.^{1,2} There is a continued search to discover novel materials that exhibit ferroelectricity. In recent years, it was discovered that specially prepared HfO₂ thin films doped with small amounts of Si (3–5 at. %) and in a mechanically compressed state exhibited a ferroelectric like behavior.³ Even more recently, HfO₂ modified with Gd, Y, Zr, and Al have also been shown to exhibit a ferroelectric-like behavior.^{4–7} Dopant concentration has been demonstrated to strongly influence the appearance of ferroelectric behavior of doped HfO₂ thin films. For example, a maximum in remnant polarization is observed for 4.3 at. % Si doping and a transition from ferroelectric to antiferroelectric behavior are observed with increasing Si-doping greater than 4.3 at. %.³

The discovery of ferroelectricity in doped HfO₂ came as a surprise because HfO₂ typically exhibits centrosymmetric crystal structures.⁸ It has been conjectured that the observation of ferroelectricity in doped HfO₂ arises from an unusual polar orthorhombic space group (*Pca2*₁) that had previously been observed in magnesia-partially stabilized zirconia.^{9–11} However, HfO₂ has not yet been confirmed as exhibiting the *Pca2*₁ space group. In fact, high-pressure X-ray diffraction (XRD) and density functional theory studies have reported that HfO₂ has two nonpolar high pressure orthorhombic polymorphs (*Pbca* and *Pmnn*).^{12–16} Recently, Huan *et al.* suggested that HfO₂ might be transformed from a nonpolar tetragonal polymorph (*P4*₂/*nmc*) into a non-centrosymmetric polymorph (*Pca2*₁ or *Pmn2*₁) by small perturbations such as electric field or stress.¹⁵

While it has been hypothesized that a polar orthorhombic polymorph is induced in doped thin films, minimal structural evidence has been reported to support the existence of the polar orthorhombic phase. For example, electron microscopy of silicon doped HfO₂ (Si:HfO₂) thin films has thus far been unable to confirm the existence of the *Pca2*₁ structure.¹⁷ Structural studies of Si:HfO₂ powders determined that Si:HfO₂ powders were monoclinic (MI) under ambient conditions.¹⁸ To provide further insight into the crystallographic structure of Si:HfO₂ and the possible role of dopant concentration on phases and phase transitions, Si:HfO₂ modified with 3, 5, or 9 at. % Si was loaded under hydrostatic compressive stresses up to 31 GPa. XRD from these powders was measured *in situ* under pressure. Measured XRD patterns were analyzed by whole pattern fitting via the Rietveld method to extract pressure-dependent structural details (space group, atomic positions, and lattice parameters).

EXPERIMENTAL METHODS

Si:HfO₂ powders with 3, 5, or 9 at. % Si-doping were prepared by standard solid-state processing. Reactant powders of HfO₂ (325 mesh, 99.95%, Alfa Aesar) and nanocrystalline SiO₂ (20–30 nm, 99.5%, Sigma-Aldrich) were reacted at 1400 °C in air for 4 h, then furnace cooled to room temperature. Further details of the processing can be found in Ref. 18. Synthesized powders were hydrostatically compressed using a diamond anvil cell (DAC). A 100 μm hole was drilled into a Rhenium (Re) gasket, then loaded with Si:HfO₂ powder and two ruby spheres for pressure calibration.¹⁹ Helium was used as a pressure-transmitting medium that provided a quasihydrostatic condition over the pressure range of interest.²⁰ Diffraction data were measured *in situ* during application of pressure at HPCAT beamline 16-BM-B ($\lambda = 0.424603 \text{ \AA}$) at the Advanced Photon Source at Argonne National Laboratory. X-ray diffraction images were

^{a)}Author to whom correspondence should be addressed. Electronic mail: jacob_jones@ncsu.edu

measured using a Mar345 image plate positioned ~ 350 cm from the sample. One-dimensional X-ray diffraction patterns were obtained by reducing measured 2-dimensional images using the FIT2D software package.²¹

Measured diffraction patterns were analyzed using the Rietveld method to extract structural details of doped HfO_2 under pressure.^{22,23} A 7th order Chebyshev polynomial background was needed to account for an irregular background that was due, in part, to transmission of the X-ray beam through the diamond. Parameters refined include the zero, profile shape, scale, phase fraction, lattice parameters, atomic positions, isotropic displacement parameters, and atomic site occupancies. The occupancies of Si and Hf were constrained to total 1.

RESULTS AND DISCUSSION

Fig. 1 shows the pressure-dependent XRD patterns of 3 at. % modified HfO_2 during application of pressure; the pressure-dependent XRD patterns for 5 and 9 at. % Si-doping are reported in Figs. S1 and S2, respectively.²⁴ Three distinct phase regions are observed during hydrostatic loading from 1 to 31 GPa for all Si concentrations: MI ($P2_1/c$), phase mixture of MI and an unidentified orthorhombic structure (OI), and OI. Undoped HfO_2 has been experimentally and theoretically shown to undergo pressure-induced transformations from MI to orthorhombic ($Pbca$) at ~ 11 GPa and from $Pbca$ to orthorhombic ($Pnma$) at 20 GPa.^{12–16} For all Si doping concentrations, OI is first observed at 7 GPa and becomes the dominant phase at ~ 10 GPa. In addition, the second high pressure orthorhombic structure (OII) (observed at ~ 20 GPa in undoped HfO_2) is not observed in Si: HfO_2 powders. This result suggests that Si modification lowers the MI to OI transition pressure (~ 7 GPa) and increases the pressure for the OI to OII transition. However, dopant concentration did not greatly impact the phase transition sequence or critical pressure to induce OI.

For 9 at. % Si: HfO_2 , the initial diffraction patterns consisted of the MI phase (as seen in 3 and 5 at. % Si: HfO_2), but also exhibited a secondary phase of crystalline SiO_2 (indexed as α -cristobalite).¹⁸ Under high pressure, crystalline SiO_2 was observed to either dissolve into solid solution or

amorphize,^{25,26} as evidenced by a reduction in the intensity and shift in the position of the α -cristobalite Bragg reflection with increased pressure, shown in Fig. S3.²⁴ Even though 9 at. % Si: HfO_2 is above the reported solubility limit of Si: HfO_2 , HfSiO_4 (the secondary phase predicted by the SiO_2 : HfO_2 phase diagram) was not observed during loading up to 30 GPa, suggesting that mechanical stress promotes the formation of (Hf,Si) O_2 solid solution.

A crystallographic structure analysis of diffraction data measured at 25 GPa was completed to identify the structure of the observed high-pressure phase of 3 at. % doped HfO_2 . Twenty-five GPa was selected because this pressure is indexed as a single orthorhombic phase. Rietveld refinements were performed using either a nonpolar orthorhombic ($Pbca$) or polar orthorhombic ($Pca2_1$) crystallographic model. Starting structural models were obtained from Ref. 15. Representative fits of the Rietveld refinements results for the $Pbca$ and $Pca2_1$ structure models are presented in Fig. S4. A summary of the refined structural parameters, atomic positions, and goodness of fit is reported in Table I. The goodness of fit suggests that the observed diffraction data are nearly equally modeled by the $Pbca$ and $Pca2_1$ structures. $Pbca$ and $Pca2_1$ can have similar diffraction patterns. However, $Pbca$ has an additional symmetry element that doubles the unit cell along the b-axis ($Pbca$, $b = 9.68423(19)\text{\AA}$; $Pca2_1$, $b = 4.84188(10)\text{\AA}$, as reported in Table I). The additional symmetry in the $Pbca$ space group results in an ordering of oxygen atoms across multiple unit cells. The oxygen ordering gives rise to additional weakly diffracting Bragg reflections, where the highest intensity superlattice peak is 0.28% of the most intense $Pbca$ reflection. Insets in Fig. S4 compare the measured and calculated intensity of the (110) reflection and $1/2(212)$ superlattice reflection.²⁴ The insets demonstrate that neither the $Pbca$ nor the $Pca2_1$ perfectly model the intensity of the superlattice reflections; the $Pbca$ structure model over estimates the intensity of the $1/2(212)$ reflection, while the $Pca2_1$ structure cannot describe the increase in intensity near this reflection.

Fig. 2 compares the log of the measured intensity of the (110) reflection and $1/2(212)$ superlattice reflection and the peak intensity for the $Pbca$ and $Pca2_1$ structures, while an

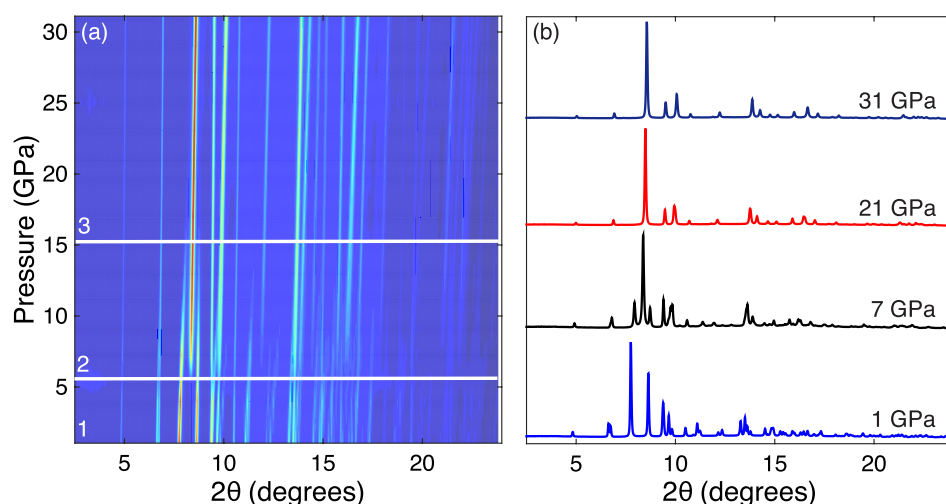


FIG. 1. Measured diffraction intensity of 3 at. % Si: HfO_2 during application of hydrostatic pressure showing three distinct phase regions; (1) MI, (2) phase mixture of MI+OI, and (3) OI. (b) Representative diffraction patterns measured at select applied pressures for each phase regime.

TABLE I. Summary of refined structural parameters, atomic positions and occupancies, and goodness of fit for Rietveld refinements using either a *Pbca* or *Pca2₁* structure model of data measured at 25 GPa.

<i>Pca2₁</i>				
	a (Å)	b (Å)	c (Å)	Profile fit
	5.12442(9)	4.84188(10)	4.85930(8)	wR _p = 2.14%
				R _p = 1.43%
				χ ² = 0.0468
	x	y	z	Occupancy
Hf	0.0336(1)	-0.2724(2)	0.242(7)	0.9700(7)
Si	0.0336(1)	-0.2724(2)	0.242(7)	0.030(4)
O(1)	0.0686(21)	-0.0557(14)	-0.284(7)	1
O(2)	-0.254(26)	-0.4748(22)	-0.015(22)	1
<i>Pbca</i>				
	a (Å)	b (Å)	c (Å)	Profile fit
	4.85919(9)	9.68423(19)	5.12461(9)	wR _p = 2.14%
				R _p = 1.45%
				χ ² = 0.0468
	x	y	z	Occupancy
Hf	0.2582(5)	0.38658(9)	-0.4663(1)	0.975(1)
Si	0.2582(5)	0.38658(9)	-0.4663(1)	0.025(1)
O(1)	0.224(7)	0.2761(8)	-0.077(2)	1
O(2)	0.520(8)	0.4942(12)	0.252(6)	1

increase in measured intensity is observed in the proximity of the $\frac{1}{2}(212)$ reflection for 3 and 5 at. % Si:HfO₂, the observed intensity is not outside of standard Poisson error ($I^{1/2}$), as shown in Fig. S5. These results suggest that OI might be *Pbca*, but the low intensity of the $\frac{1}{2}(212)$ peak prevents ascribing OI to a specific space group. Furthermore,

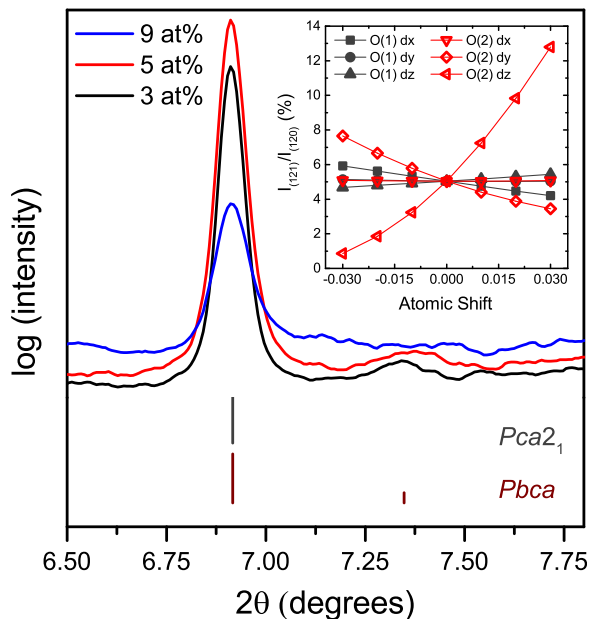


FIG. 2. Comparison of measured diffraction profiles in Si doped HfO₂ powders measured at 25 GPa and tick marks that are representative the position and intensity of the (110) reflections and $\frac{1}{2}(212)$ superlattice reflection. Diffraction profiles and peak intensity marks are plotted in log scale to illustrate that the intensity of the $\frac{1}{2}(212)$ superlattice reflection is weak. The inset shows the intensity ratio of the $\frac{1}{2}(212)$ and (110) reflections for various x, y, and z perturbations from the refined atomic positions of the two degenerate oxygen of *Pbca*.

Fig. 2 illustrates the difficulty in proving the existence of the superlattice reflection. The inset in Fig. 2 compares the intensity ratio of the $\frac{1}{2}(212)$ superlattice and $\frac{1}{2}(212)$ reflection for various x, y, and z shifts from the refined atomic position for the two degenerate oxygen positions of *Pbca*. The inset in Fig. 2 indicates that small perturbations in the oxygen atomic positions, specifically the y and z position of O(2), influence the intensity of the superlattice reflection. For example, a perturbation in the z position of O(2) by the estimated standard deviation (± 0.006) would have an appreciable impact on the intensity, further indicating that there is minimal confidence in the intensity of the superlattice reflection.

The low atomic scattering factor of oxygen relative to hafnium (1:9) complicates the detection of the superlattice reflection using XRD. Neutrons, on the other hand, offer more sensitivity to oxygen in the presence of hafnium. Ohtaka *et al.* observed a spurious reflection in neutron diffraction patterns of ZrO₂ quenched from high pressure (6 GPa) and temperature (600 °C) that could not be accurately modeled using previously reported structures of *Pbcm*, *Pbam*, or *Pba2₁*.²⁷ The observed reflection was accurately described by a *Pbca* phase, and was attributed to ordering of oxygen atoms. Howard *et al.* also used neutron diffraction to determine that the low temperature crystallographic structure of magnesia-partially stabilized zirconia was *Pca2₁*.

Pressure dependent lattice parameters of MI and OI were obtained by whole pattern fitting. The MI and OI structures were modeled using *P2₁/c* and *Pca2₁* space groups, respectively. OI was modeled using the *Pca2₁* space group because it is the simpler of the two OI models. It is noted that diffraction signal from MI persisted up to 21 GPa, but peak overlap with OI and the small volume fraction of MI prevented reliable lattice parameter measurements. Fig. 3 shows the measured lattice parameters for the *P2₁/c* (a_M , b_M , c_M , and β_M) and *Pca2₁* (a_O , b_O , and c_O) structures over the applied pressure range. With increasing pressure, the lattice parameters of MI and OI appear a continuous along the b_M+a_O and a_M+c_O crystallographic directions. Fig. 3 suggests that Si concentration has minimal or no influence on the measured lattice parameters.

The relative volume of MI and OI was calculated to elucidate additional information about the effect of Si on the observed high-pressure structures. Fig. 4 displays the relative volume of Si:HfO₂ for the MI and OI phases. Increasing applied pressure induces a greater reduction in volume for the MI phase than OI phase, indicating that MI is elastically softer than OI. This result is consistent with both experiment and theoretical studies, which have reported that the high-pressure orthorhombic structures of HfO₂ are elastically harder and have a higher bulk modulus than MI.^{12-14,16,28} From Fig. 4, it is also apparent that Si concentration has a negligible impact on the high-pressure structures of HfO₂.

The structural data can also be used to extract spontaneous strain (S), which is a scalar representation of the spontaneous ferroelastic strain tensor. S of MI and OI was calculated using the methodology reported in Ref. 18, and is shown in Fig. 4. For all Si concentrations, the S of MI was found to decrease with pressure, while the S of OI increased.

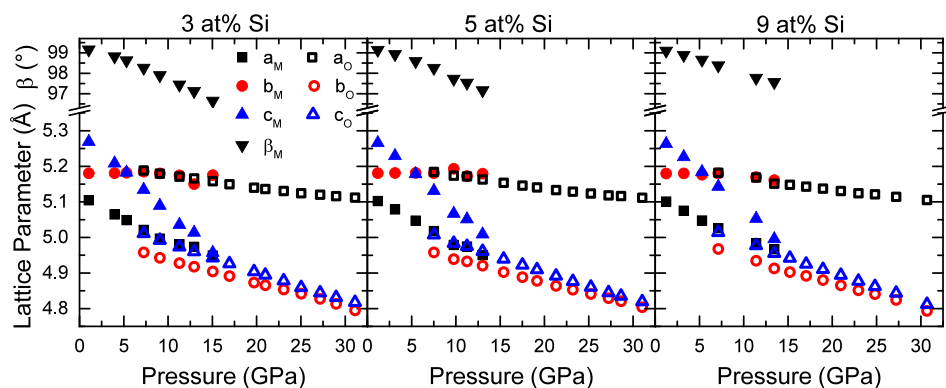


FIG. 3. Pressure-dependent unit cell parameters of the MI (solid) and OI (open) phases in Si:HfO₂ over the pressure range of interest. Note that increased Si concentration does not strongly influence the pressure dependent structure of HfO₂. Error bars are smaller than symbols.

The reduction in S of MI with pressure is an indication that the MI becomes less distorted, as evident by a substantial decrease of the monoclinic distortion angle (β_m). An increase in S of OI is attributed to the anisotropic compressibility of the principle axis of OI, where the reduction in a_O with pressure ($da_O/dP = -0.30$ pm/GPa) is less than that of b_O ($db_O/dP = -0.64$ pm/GPa) and c_O ($dc_O/dP = -0.79$ pm/GPa), as illustrated in Fig. 3.

It has been previously suggested that the observed antiferroelectric-like polarization behavior of doped HfO₂ thin films arises from a reversible field-induced transition from nonpolar (tetragonal $P4_2/nmc$) to polar ($Pca2_1$).^{29,30} In the present work, a tetragonal polymorph was not detected for 5 or 9 at. % Si:HfO₂, suggesting that the observed transition in doped HfO₂ thin films from ferroelectric to antiferroelectric behavior does not arise from the combination of chemical doping and hydrostatic pressure. Instead, the present results are consistent with an alternative hypothesis that a more complex stress state imposed by biaxial film stresses might have a greater effect on the crystallographic structure than hydrostatic stress. For example, such biaxial film stresses could arise from thermal expansion mismatch between the substrate:HfO₂ and HfO₂:capping layer.

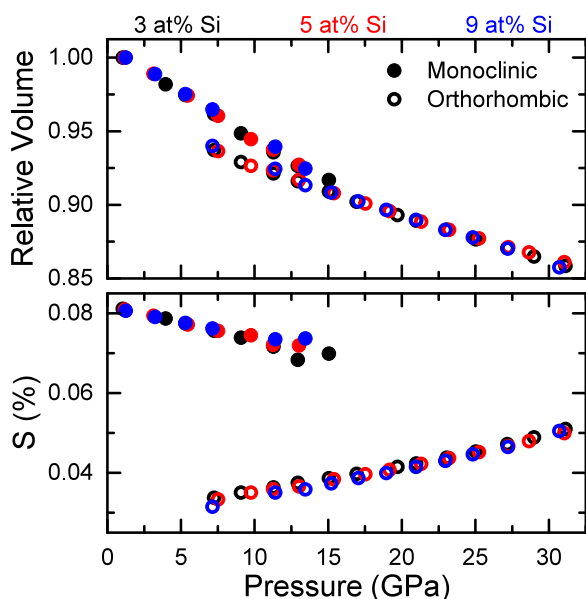


FIG. 4. Pressure induced change in relative volume (top) and spontaneous strain (bottom) of the observed MI (solid) and OI (open) for 3 (black), 5 (red), and 9 (blue) at. % Si:HfO₂. Error bars are smaller than symbols.

CONCLUSION

In summary, the pressure induced structures of Si:HfO₂ were determined. The observed phase transformation pressures of Si:HfO₂ were found to be different than pure HfO₂. A crystallographic structure analysis was undertaken using $Pbca$ and $Pca2_1$ structure models to determine the symmetry of the high-pressure OI structure of Si:HfO₂. The structural analysis using synchrotron X-ray diffraction is unable to reliably discriminate between $Pbca$ and $Pca2_1$ structure models. Si-doping concentration was found to have minimal impact on the pressure dependent lattice parameters, suggesting that the combination of Si doping and pressure cannot explain the origin of the ferroelectric to antiferroelectric transition observed in Si:HfO₂ thin films.

ACKNOWLEDGMENTS

Portions of this work were performed at HPCAT (Sector 16), Advanced Photon Source (APS), Argonne National Laboratory. HPCAT operations are supported by DOE-NNSA under Award No. DE-NA0001974, and DOE-BES under Award No. DE-FG02-99ER45775 with partial instrumentation funding by NSF. The Advanced Photon Source is a U.S. Department of Energy (DOE) Office of Science User Facility operated for the DOE Office of Science by Argonne National Laboratory under Contract No. DE-AC02-06CH11357.

- ¹L. E. Cross, *Mater. Chem. Phys.* **43**, 108 (1996).
- ²J. Rödel, W. Jo, K. T. P. Seifert, E. M. Anton, T. Granzow, and D. Damjanovic, *J. Am. Ceram. Soc.* **92**, 1153 (2009).
- ³T. S. Böske, J. Müller, D. Bräuhäus, U. Schröder, and U. Böttger, *Appl. Phys. Lett.* **99**, 102903 (2011).
- ⁴S. Müller, C. Adelman, A. Singh, S. Van Elshocht, U. Schröder, and T. Mikolajick, *ECS J. Solid State Sci. Technol.* **1**, N123 (2012).
- ⁵S. Müller, J. Müller, A. Singh, S. Riedel, J. Sundqvist, U. Schröder, and T. Mikolajick, *Adv. Funct. Mater.* **22**, 2412 (2012).
- ⁶J. Müller, U. Schröder, T. S. Böske, I. Müller, U. Böttger, L. Wilde, J. Sundqvist, M. Lemberger, P. Kücher, T. Mikolajick, and L. Frey, *J. Appl. Phys.* **110**, 114113 (2011).
- ⁷M. Hyuk Park, H. Joon Kim, Y. Jin Kim, W. Lee, T. Moon, and C. Seong Hwang, *Appl. Phys. Lett.* **102**, 242905 (2013).
- ⁸O. Ohtaka, H. Fukui, T. Kunisada, T. Fujisawa, K. Funakoshi, W. Utsumi, T. Irifune, K. Kuroda, and T. Kikegawa, *J. Am. Ceram. Soc.* **84**, 1369 (2001).
- ⁹C. J. Howard, E. H. Kisi, and O. Ohtaka, *J. Am. Ceram. Soc.* **74**, 2321 (1991).
- ¹⁰E. H. Kisi, C. J. Howard, and R. J. Hill, *J. Am. Ceram. Soc.* **72**, 1757 (1989).
- ¹¹C. J. Howard, E. H. Kisi, R. B. Roberts, and R. J. Hill, *J. Am. Ceram. Soc.* **73**, 2828 (1990).

- ¹²J. M. Leger, P. E. Tomaszewski, A. Atouf, and A. S. Pereira, *Phys. Rev. B* **47**, 14075 (1993).
- ¹³J. Lowther, J. Dewhurst, J. Leger, and J. Haines, *Phys. Rev. B* **60**, 14485 (1999).
- ¹⁴Y. Al-Khatatbeh, K. K. M. Lee, and B. Kiefer, *Phys. Rev. B* **82**, 144106 (2010).
- ¹⁵T. D. Huan, V. Sharma, G. A. Rossetti, and R. Ramprasad, *Phys. Rev. B* **90**, 064111 (2014).
- ¹⁶J. Kang, E.-C. Lee, and K. Chang, *Phys. Rev. B* **68**, 054106 (2003).
- ¹⁷P. D. Lomenzo, P. Zhao, Q. Takmeel, S. Moghaddam, T. Nishida, M. Nelson, C. M. Fancher, E. D. Grimley, X. Sang, J. M. LeBeau, and J. L. Jones, *J. Vac. Sci. Technol., B* **32**, 03D123 (2014).
- ¹⁸L. Zhao, M. Nelson, H. Aldridge, T. Iamsasri, C. M. Fancher, J. S. Forrester, T. Nishida, S. Moghaddam, and J. L. Jones, *J. Appl. Phys.* **115**, 034104 (2014).
- ¹⁹H. K. Mao, J. Xu, and P. M. Bell, *J. Geophys. Res.* **91**, 4673, doi:10.1029/JB091iB05p04673 (1986).
- ²⁰T. Kenichi, *J. Appl. Phys.* **89**, 662 (2001).
- ²¹A. P. Hammersley, S. O. Svensson, M. Hanfland, A. N. Fitch, and D. Hausermann, *High Pressure Res.* **14**, 235 (1996).
- ²²A. C. Larson and R. B. Von Dreele, Los Alamos National Laboratory Report No. LAUR 86-748 (2004).
- ²³B. H. Toby, *J. Appl. Crystallogr.* **34**, 210 (2001).
- ²⁴See supplementary material at <http://dx.doi.org/10.1063/1.4922717> for pressure dependent diffraction patterns of 5 and 9 at.% Si:HfO₂ and representative Rietveld refinement results.
- ²⁵S. M. Sharma and S. K. Sikka, *Prog. Mater. Sci.* **40**, 1 (1996).
- ²⁶X. Zhang and C. K. Ong, *Phys. Rev. B* **48**, 6865 (1993).
- ²⁷O. Ohtaka, T. Yamanaka, and S. Kume, *Proc. Jpn. Acad., Ser. B* **66**, 193 (1990).
- ²⁸S. Desgreniers and K. Lagarec, *Phys. Rev. B* **59**, 8467 (1999).
- ²⁹S. Reyes-Lillo, K. Garrity, and K. Rabe, *Phys. Rev. B* **90**, 1 (2014).
- ³⁰T. S. Böske, S. Teichert, D. Bräuhäus, J. Müller, U. Schröder, U. Böttger, and T. Mikolajick, *Appl. Phys. Lett.* **99**, 112904 (2011).